This is the final draft of the contribution published as:

The publisher's version is available at:

1 **Electric Field Effects on Bacterial Deposition and Transport in Porous Media**

2

3 Yongping Shan, Hauke Harms, and Lukas Y. Wick*

4

5

6

7

8 *UFZ - Helmholtz Centre for Environmental Research, Department of Environmental*
9 *Microbiology, 04318 Leipzig, Germany*

10

11

12

13 Running title: Electric field effects on bacterial deposition and transport in porous media

14 Intended for: Environmental Science and Technology

15

16

17

18

19

20

21

22 * Corresponding author: Mailing address: Helmholtz Centre for Environmental Research - UFZ.
23 Department of Environmental Microbiology; Permoserstrasse 15; 04318 Leipzig, Germany.
24 phone: +49 341 235 1316, fax: +49 341 235 45 1316, e-mail: lukas.wick@ufz.de.

Abstract

Bacterial deposition and transport is key to microbial ecology and biotechnological applications. We therefore tested whether electrokinetic forces (electroosmotic shear force (F_{EOF}), electrophoretic drag force (F_{EP})) acting on bacteria may be used to control bacterial deposition during transport in laboratory percolation columns exposed to external direct current (DC) electric fields. For different bacteria, yet similar experimental conditions we observed that DC fields either enhanced or reduced bacterial deposition efficiencies (α) relative to DC-free controls. By calculating the DLVO force of colloidal interactions, F_{EOF}, F_{EP}, and the hydraulic shear forces acting on single cells at a collector surface we found that DC-induced changes of α correlated to $\left| F_{EOF} \right|$ to $\left| F_{EP} \right|$ ratios: If $\left| F_{EOF} \right| > \left| F_{EP} \right|$, α was clearly increased and if $\left| F_{EOF} \right| < \left| F_{EP} \right|$ α was clearly decreased. Our findings allow for better prediction of the forces acting on a bacterium at collector surface and, hence, the electrokinetic control of microbial deposition in natural and manmade ecosystems.
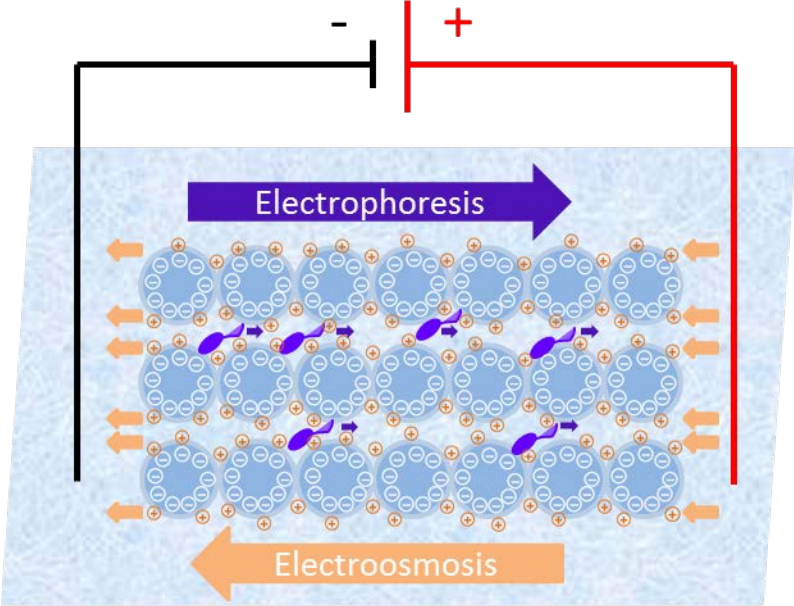
44   **TOC**

45

Electrophoresis

Electroosmosis

46

47

Introduction

Transport and deposition of bacteria are fundamental processes in microbial ecology and biotechnology[1]. They enable microbial functions in disturbed systems[2] or promote the formation of biofilms as a major life form of bacteria. While the catabolic activity of biofilms provide essential ecosystem services in natural and manmade systems (e.g. for the degradation of anthropogenic chemicals or in waste water treatment), biofouling[3] by contrast may give rise to unwanted corrosion of metals[4], clogging of filters/membranes or may even threaten human health by infecting medical devices[1] or technical systems for the provision of drinking water. There is, hence, strong interest in measures to control microbial deposition to surfaces as the first step in the formation of biofilms. Bacterial deposition is influenced by physicochemical properties of the microbe, the collector surface, and the aqueous medium[5]. Deposition to collector surfaces during transport in porous systems can be suitably approximated by the collision efficiency α_t and clean-bed filtration theory[6,7], while the distance-dependent energy between a bacterium and a collector surface (G_{DLVO}) can be quantified by the Derjaguin, Landau, Verwey, and Overbeek (DLVO) theory[8]. As the deposition of a bacterium requires that its kinetic energy is lower than its interaction energy with a collector surface, α_t normally is positively correlated to G_{DLVO} at the distance of reversible attachment (i.e. at the secondary minimum of G_{DLVO})[9]. Although the DLVO theory refers to an ideal system (i.e. does not encompass heterogeneities in surface charge[10,11], surface roughness[12], hydration effects, or hydrophobic interaction[8,13]), it has been found to be a powerful predictor of bacterial deposition in solutions of high ionic strength (I = 0.1 - 0.3 M)[9,10,14] and/or to highly uniform surfaces of low surface roughness.

70   The electric field-induced phenomena electroosmosis and electrophoresis have been found to be

71   powerful tools in controlling the movement of bacteria and (bio-)colloidal particles[15–18]. When a

72   DC electric field is applied to an ionic solution in a solid matrix, it invokes various electrokinetic

73   transport processes: Electromigration and electrophoresis denote the transport of charged

74   molecules and particles, to the electrode of opposite charge, while electroosmotic flow (EOF)

75   refers to the surface charge-induced movement of pore fluids usually from the anode to the

76   cathode[19]. Due to its plug shape flow profile, EOF has been found to be efficient at a distance of

77   a few nanometers above the solid surface where bacterial deposition interaction takes place and

78   thus significantly affects bacterial deposition efficiency[20]. Both phenomena are directly

79   correlated to the electric field strength applied and allow for the movement of bacteria and

80   colloidal particles[15–18] in porous media also in the absence of a pressure-driven hydraulic flow[21–

81   23] or for the separation of monoclonal bacteria differing in the zeta potentials[24].

82   Inspired by such observations, recent work compared the DLVO forces (F_{DLVO}), electroosmotic

83   shear force (F_{EOF}), and hydraulic shear force (F_{HF}) acting on a bacterium at the secondary

84   minimum distance and described F_{EOF} as a relevant driver for the reduction of the initial

85   adhesion of *Pseudomonas fluorescens* LP6a[20]. This approach, however neglected the

86   electrophoretic drag force (F_{EP}) acting on bacteria and hence was unable to predict the interplay

87   of F_{EOF}, F_{EP}, and F_{DLVO}. Here we experimentally quantify the effect of DC fields on the transport

88   and deposition of four bacteria differing in their surface charge (zeta potential) and

89   hydrophobicity in percolation columns. The observed DC field effects on bacterial deposition

90   efficiencies (α_t) relative to DC-free controls are reflected by calculations of the net force acting

91   on a bacterium at secondary minimum distance by F_{EOF}, F_{EP}, F_{HF}, and F_{DLVO}.

92

Materials and Methods

Cultivation of Bacteria and Preparation of Inocula

Pseudomonas putida KT2440 (GenBank accession No. AE015451)[25], *Rhodococcus opacus* X9 (GenBank accession No. AF095715)[26], *Pseudomonas fluorescens* LP6a (GenBank accession No. AF525494)[27] and *Sphingomonas* species S3 (GenBank accession No. MH048882) were cultivated in 500-mL Erlenmeyer flasks using 200 mL of minimal medium containing 1.0 g L^{-1} glucose (25 °C, rotary shaker at 150 rpm). The cultures were harvested in the early stationary phase (i.e. after 14 h for strain *P. putida* KT2440, 15 h for strain *R. opacus* X9, 12 h for strain *P. fluorescens* LP6a, and 7 d for strain *Sphingomonas* sp. S3, centrifuged at 3000 × g and re-suspended in 100 mM potassium phosphate buffer (PB, pH = 7, prepared by adding 0.061 mol K_2HPO_4 and 0.039 mol KH_2PO_4 in 1 L deionized water) with a Vortex mixer (Vortex-Genie 2, Scientific Industries, USA) to obtain an optical density of $OD_{600\ nm}$ = 0.30 using an UV/VIS Spectrophotometer (Evolution 160, Thermo Fisher Scientific, USA).

Characterization of Physico-Chemical Surface Properties of Bacteria and Glass Beads

The zeta potential (ζ) of bacteria and smashed glass beads were measured by Doppler electrophoretic light scattering analysis (Zetamaster, Malvern Instruments, Malvern, UK, with a Dip Cell Kit or a Folded Capillary Cell) in 100 mM PB (pH = 7). In deviation from an earlier described procedure[20] analyses were performed at 60 V in order to obtain narrow and symmetrical signal peaks. To approximate the effect of bacterial deposition on the zeta potential of glass beads (0.1 − 0.25 mm diameter, Retsch, Germany), clean polished glass beads were smashed with a mortar and a pestle to a size of < 100 µm, then heated at 200 °C in muffle furnace for 2 hours, allowed to cool down to room temperature (25 °C) under sterile conditions and then immersed during 2 hours to the bacterial suspensions ($OD_{600\ nm}$ = 0.30). The beads then

116 were separated by sieving, rinsed cautiously with 100 mM PB, re-suspended in 100 mM PB and

117 analyzed as described above. Glass beads that were treated identically yet not exposed to

118 bacterial cells were measured to obtain the ζ of the clean bed (i.e. collector) surfaces. The contact

119 angles (Θ) of the bacteria were measured using a DSA 100 drop-shape analysis system (Krüss

120 GmbH, Hamburg, Germany) using water (Θ_w), formamide (Θ_f), and methylene iodide (Θ_m) as

121 described earlier[20]. Bacterial lawns were prepared by depositing bacteria from inoculated

122 suspensions on cellulose acetate membrane filters (Millipore, 0.45 μm). 9 bacterial lawns were

123 prepared for each bacterial cultivation to perform triplicate experiments for each solvent, 4

124 droplets were applied on each bacterial lawn (i.e. the contact angle in each solvent is an average

125 of 12 droplets). Glass bead lawns were prepared by fixing (either clean or bacteria-covered) glass

126 beads with double-sided tape to glass slides by gentle pressing as described by Achtenhagen et

127 al[28]. Glass beads of similar bacterial coverage as calculated for conditions of late stage

128 breakthrough curves (cf. Tables 2 & S6 and Figs. 1 & S2) were prepared as described in the SI.

129 The contact angles of the glass beads are averages of 12 droplets).

Column Deposition Experiments

131 The breakthrough curves of the different strains were quantified in vertical percolation columns

132 as described by Qin et al[20]. Shortly, the columns were sterilized and packed with clean, heat-

133 sterilized (200 ^{o}C, 2 h) polished glass beads, the porosity and pore volume (PV) were estimated

134 to be 0.42 and 3.97 mL, respectively. Two disk-shaped Ti/Ir electrodes (De Nora Deutschland

135 GmbH, Germany) at the top (cathode) and bottom (anode) of the column were connected to a

136 power pack (P333, Szczecin, Poland) that allowed to apply constant DC electric field at $E = 0$

137 (control), 0.5, 1.0, 1.5, 2.0, 2.5, or 3.0 V cm^{-1}. The columns were allowed to equilibrate by

138 circulating clean buffer (100 mM PB, $I = 0.22$ M) for 30 min. Well stirred bacterial suspensions

139 were allowed to percolate through the columns at a hydraulic flow rate of 19.3 mL h^{-1} (flow

140 velocity: 2.4 × 10^{-7} m s^{-1}) from the top to the bottom using a peristaltic pump. By placing the

141 anode at the outflow of the column potential impacts of anodic reactive oxygen species on

142 bacterial deposition were avoided. The lid at the top of the column permitted the release of

143 electrolytically formed gas bubbles and, hence, avoided the passage of gas bubbles through the

144 packed bed. For some strains (*P. putida* KT2440, *P. fluorescens* LP6a) additional experiments

145 with reversed electrode polarity (top: anode; bottom: cathode) at $E = 2$ V cm^{-1} were performed.

146 The deposition of cells was determined by comparing the OD$_{600\ nm}$ of the influent (C$_0$) and

147 effluent (C).

148 **Theory**

149 **Calculation of Collision Efficiency**

150 Clean-bed filtration theory was used to quantify the bacterial deposition in the glass beads

151 packed columns in the presence and absence of electric fields. The collision efficiency α_t is

152 described by[6,7]

153 $$\alpha_t = \frac{\eta_t}{\eta_{trans}} \tag{1}$$

154 with η_t being the rate of attachment as calculated from bacterial breakthrough data and η_{trans} the

155 rate of bacteria transport to the collector surfaces, the calculation method has been described in

156 detail by Qin et al.[20] and in the SI.

157

158 **Prediction of Forces Acting on a Cell at the Secondary Minimum above a Collector Surface**

159 According to the DLVO theory, the DLVO energy distribution (G_{DLVO}, eq. 2)[8] is composed of

160 the electrostatic (G_{EDL}) and Lifshitz−van der Waals (G_{LW}) energies (for detailed description

161 please refer to the SI). The zeta potentials and contact angles of bacterial and collector surfaces,

162 respectively, were used to approximate the overall DLVO interaction energies; Calculations of

163 G_{DLVO} thereby considered changes of the zeta potential and the contact angles of the collector

164 surface in response to increasing bacterial deposition (for detailed description of the effects of

165 bacterial coverage on the zeta potential and contact angles of the collectors refer to the SI; eqs.

166 S9-S15, Table S6, and Fig. S5).

167 $$G_{DLVO} = G_{EDL} + G_{LW} \qquad (2)$$

168 At the secondary minimum distance (h_s) to a collector surface, F_{DLVO} (eq. 3) can be calculated by

169 the DLVO energy distribution (G_{DLVO})[8]:

170 $$F_{DLVO} = \frac{G_{DLVO}}{h_s} \qquad (3)$$

171 The resulting net force (F_{net}) acting on a bacterium located at the distance of the secondary

172 minimum above a collector surface submersed in an ionic solution in presence of an external DC

173 electric field can be approximated by combination of shear forces induced by the hydraulic (F_{HF}),

174 and the electroosmotic (F_{EOF}) water flow and the electrophoretic drag force (F_{EP}) in eq 4:

175 $$F_{net} = F_{EOF} + F_{EP} + F_{HF} + F_{DLVO} \qquad (4)$$

176 The shear forces F_{HF} and F_{EOF}, acting on a bacterium located at h_s depend on the velocity of the

177 hydraulic (V_{HF}) and the electroosmotic (V_{EOF}) water flow and can be calculated by eqs. 5 & 6[29]:

178 $$F_{HF} = F_d^* \times 6\pi\eta a V_{HF} \qquad (5)$$

179 $$F_{EOF} = F_d^* \times 6\pi\eta a V_{EOF} \qquad (6)$$

180 Where η is the viscosity of the liquid ($\eta = 3.19$ kg m^{-1} h^{-1}), F_d^* is a function of the radius a of a

181 sphere (for simplicity we presume bacterial cells to be spheres) and the distance of the center of

182 the sphere to the collector surface. Following previous work we presume F_d^* to be 1.7[29]. The

183   velocity of hydraulic flow can be described by the Hagen-Poiseuille approach[30]. The EOF

184   velocity (V_{EOF}) at distance h_s from the collector surface is calculated by eq. 7, which is the

185   combination of a simplified EOF expression of the Navier-Stokes equation with the potential

186   distribution described by the Gouy-Chapman model, and the characteristics of porous media

187   were taken into account[20,31,32].

188 $$V_{EOF} = -\frac{\varepsilon_0 \varepsilon_r \zeta_C n\tau * E}{\eta}\left(1 - \frac{2I_1(\kappa h_s)}{\kappa a I_0(\kappa h_s)}\right) \tag{7}$$

189   In eq. 7 ε_r is the dielectric constant of water (78.5), ε_0 (8.85×10^{-12} F m^{-1}) is the vacuum

190   permittivity, ζ_C is the zeta potential of the collector surface at the experimental conditions, n and

191   τ refer to the porosity (0.42) and tortuosity (1.8) of the glass bead bed[32], and E is the electric field

192   strength applied, I_0 and I_1 are the zero- and first-order modified Bessel functions, and κ^{-1} is the

193   thickness of the electric double layer. The drag force F_{EP} acting on a bacterium is calculated

194   from the electrophoretic mobility V_{EP} according to Solomentsev et al.[30,33].

195 $$F_{EP} = 6\pi\eta a V_{EP} \tag{8}$$

196   The electrophoretic velocity (V_{EP}) is calculated by the Smoluchowski equation[34]

197 $$V_{EP} = \frac{2\varepsilon_0 \varepsilon_r \zeta_{bac} E}{3\eta} f_{(\kappa a)} \tag{9}$$

198      $f(\kappa a)$ approaches 1 for small κa, and 1.5 for large κa, here $f(\kappa a)$ value level off to 1.5[35]. The ratio

199   of F_{EOF} and F_{EP} is given by eq. 10

200 $$\frac{F_{EOF}}{F_{EP}} = \frac{F_d {}^* \zeta_C n\tau}{\frac{2}{3} * \zeta_{bac} f(\kappa a)}\left(1 - \frac{2I_1(\kappa h_s)}{\kappa a I_0(\kappa h_s)}\right) = 1.29 * \frac{\zeta_C}{\zeta_{bac}} \tag{10}$$

201

Results

Quantification of Cell Deposition in Percolation Columns

The effects of DC electric fields on bacterial deposition and transport of *P. putida* KT2440, *R. opacus* X9, *P. fluorescens* LP6a, and *Sphingomonas* sp. S3 were quantified in percolation columns filled with glass beads at various electric field strengths (E = 0 - 3.0 V cm^{-1}). By quantifying relative effluent cell densities, the breakthrough curves of DC and DC-free columns were compared and clean bed theory was adopted to describe the bacterial deposition. The collision efficiency of the clean bed (i.e. at the initial stage of bacterial breakthrough; α_0) was evaluated from data of 0 - 2 PV of the breakthrough curves (Table 1, Figs. 1, S1 & S3), while later stage collision efficiencies (α_t) were obtained from the breakthrough curves at quasi steady state (Table 1, Figs. 1 & S2). All four bacterial strains differed in their physico-chemical surface properties. In the percolation buffer they exhibited zeta potentials (ζ_{bac}) of -11 to -35 mV (Table 1). All strains were moderately hydrophobic with water contact angles varying between 46° - 70°. Such differences were also reflected by distinct breakthrough curves in DC-free controls: strains KT2440 and X9 were less retained than strains LP6a and S3 (Table 1); this is reflected by smaller collision efficiencies ($\alpha_t \approx 0.004 – 0.01$ vs. 0.02; Table 1) and lower fractions of retained bacteria after 14 PV ($\approx$ 4 % vs. 10 – 14 %, Fig. 1). No significant differences of the clean bed collision efficiencies ($\alpha_0 \approx 0.3 – 0.4$), however, were calculated. The zeta potential of the glass beads (ζ_C) changed from -8 mV (clean bed) to ca. -11– -16 mV (ζ_{C_t}, Table 1) in response to bacterial deposition (surface coverage of 4 % – 14 % (Table S6)). Bacterial deposition likewise changed the contact angle of clean glass beads ($\Theta_w = 21^o$) to 25° (*P. putida* KT2440), 30° (*R. opacus* X9), 34° (*P. fluorescens* LP6a) and 39° (*Sphingomonas* sp. S3) (Tables 1 & S6).

224   Applying DC fields to the columns resulted in changed breakthrough of all four strains.

225   Observed effects depended on the electric field strengths applied and the zeta potential of the

226   bacterial (ζ_{bac}) and the glass bead surfaces (ζ_C and ζ_{C_t}): At $\zeta_{bac} / \zeta_C \gtrsim 1.29$ the DC fields led to a

227   decreased bacterial deposition, while at $\zeta_{bac} / \zeta_C \lesssim 1.29$ DC fields promoted bacterial deposition

228   to the glass collector surfaces. Both the positive and negative DC effects on bacterial deposition

229   increased at augmenting field strengths (Table 1 & Fig. 1 for E = 0, 1, 2, and 3 V cm^{-1}; Fig. S1

230   and Table S2 for E = 0.5, 1.5, and 2.5 V cm^{-1}). Applying DC fields to the columns hence

231   decreased bacterial initial deposition for all strains at < 2 PV. This resulted, for instance, in

232   decreases of α_0 at E = 3V cm^{-1} by 85 % (LP6a), 68 % (S3), 65 % (X9), and 32 % (KT2440)

233   relative to DC-free controls. At > 2 PV bacterial breakthrough showed two distinct tendencies:

234   the presence of DC clearly decreased deposition of strains S3 and LP6a, as exemplified by 40-

235   100 % reduced α_t at E = 3 V cm^{-1} (Tables 1 & S2, Figs. 1 & S1). By contrast, up to 584 %

236   increased collision efficiencies α_t of strains KT2440 and X9 were observed at E = 3 V cm^{-1}

237   (Table 1, Fig.1).

238   **Net Forces Acting on a Cell Placed at the Distance of the Secondary Minimum**

239   Tables 2 (E = 0, 1, 2, 3 Vcm^{-1}) & S3 (E = 0, 0.5, 1.5, 2.5 Vcm^{-1}) summarize the net forces (F_{net},

240   cf. eq. 4) acting on bacteria placed at the distance of the secondary minimum above a collector

241   surface in presence and absence of DC electric fields of varying field strengths; i.e. the DLVO

242   force (F_{DLVO}, cf. eq. 3), the hydraulic (F_{HF}, cf. eq. 5) and electroosmotic shear forces (F_{EOF}, cf.

243   eq. 6 & 7), and the electrophoretic drag force (F_{EP}, cf. eq. 8 & 9). The F_{DLVO} ranged from 1.83 to

244   9.82 pN and, the distance of the secondary minimum (cf. Fig. S5 & Table S6), were significantly

245   higher than strain-independent F_{HF} = 0.2 pN. The DLVO approach was used as it has been found

246   to be a powerful predictor of bacterial deposition to chemically uniform collector surfaces of

247 poor surface roughness immersed in solutions of high ionic strength (I = 0.1 - 0.3 M), i.e.

248 conditions as given in our experiments.

249 As both the bacterial and the glass collector surfaces were measured to be negatively charged

250 (Table 1), the electrophoretic drag forces F_{EP} and the electroosmotic shear force counteracted

251 each other (as expressed by opposite signs of the forces) and depended on the electric field

252 strength applied. For situations of clean bed surfaces (ζ_C = -8 mV), $|F_{EOF}|$ < $|F_{EP}|$ was

253 calculated for all strains and all conditions tested (Table 2). In such situation and in presence of

254 DC F_{net} was consistently < F_{DLVO} and allowed for less bacterial deposition (i.e. decreasing α_0 or

255 better bacterial transport) than in DC-free controls. Due to the deposition-induced increase of the

256 zeta potential (ζ_{C_t}) of the collector surfaces, the velocity of the EOF (V_{EOF}; eq. 7) increased

257 during percolation. This resulted in an increased F_{EOF} yet let F_{EP} unchanged. For strains LP6a

258 and S3 $|F_{EOF}|$ remained < $|F_{EP}|$ while for strains KT2440 and X9 $|F_{EOF}|$ became > $|F_{EP}|$.

259 As a consequence F_{net} remained < F_{DLVO} for strains LP6a and S3 yet at E = 3 V cm^{-1} increased

260 by 29 % and 5 % for strains KT2440 and X9 relative to F_{DLVO} (Tables 2 & S3).

261

262 **Discussion**

263 **Drivers of Deposition Efficiencies and Net Forces at the Secondary Minimum**

264 Inspired by previous work[20] that interlinked reduced deposition efficiencies of *P. fluorescens*

265 LP6a cells with electroosmotic shear forces (F_{EOF}) in electrokinetic percolation columns we here

266 challenged the proposed F_{EOF}-effects by quantifying deposition and transport of four soil bacteria

267 differing in their physico-chemical cell surfaces and deposition properties. While our data

268 confirm deposition-limiting F_{EOF}-effects for LP6a cells (i.e. that F_{EOF} are able to overcome the

269   F_{DLVO}), we simultaneously found that DC electric fields promoted the deposition of *P. putida*

270   KT2440 and *R. opacus* X9 up to 584 % and 66 % despite of $\left| F_{EOF} \right| \geq \left| F_{DLVO} \right|$ (Table 2). In

271   order to explain such discrepancy we included the electrophoretic drag force, F_{EP} as additional

272   driver of the F_{net} (eq. 4) acting on a cell sitting at the distance of the secondary minimum (eq. 4)

273   above a glass bead collector surface. We found that the relative changes of DC-induced net

274   forces (expressed by $(F_{net,DC} - F_{net,noDC}) / F_{net,noDC}$) were highly correlated with the relative

275   changes of the collision efficiency (expressed by $(\alpha_{DC} - \alpha_{noDC}) / \alpha_{noDC}$) (Fig. 3). At conditions of

276   $F_{net,DC} > F_{net,noDC}$ (i.e. $\left| F_{EOF} \right| > \left| F_{EP} \right|$) increased deposition, while for $F_{net,DC} < F_{net,noDC}$ (i.e.

277   $\left| F_{EOF} \right| < \left| F_{EP} \right|$) decreased deposition was detected for all bacteria and all stages of the

278   breakthrough curves. Comparison of the absolute values of F_{EOF} and F_{EP} (Table 2) reveals that at

279   $\left| F_{EOF} \right| > \left| F_{EP} \right|$ improved and at $\left| F_{EOF} \right| < \left| F_{EP} \right|$ reduced bacterial deposition relative to

280   DC-free controls was observed. Our data hence suggest that electrokinetic shear and drag forces

281   are drivers of electrokinetic influences on bacterial deposition. As both forces are influenced by

282   the same drivers (e.g. electric field strength and the thickness of the electric double layer), the

283   $\left| F_{EOF} / F_{EP} \right|$ ratio can be expressed in a given medium in function of the zeta potentials of the

284   bacteria and the collector surface by $1.29 * \zeta_C / \zeta_{bac}$ (eq.10): at $1.29 * \zeta_C / \zeta_{bac} < 1$ reduced

285   deposition ($\alpha_{DC} < \alpha_{noDC}$) and at $1.29 * \zeta_C / \zeta_{bac} > 1$ increased deposition ($\alpha_{DC} > \alpha_{noDC}$) is to be

286   predicted (Fig. 2). The zeta potential ratio between collector and bacteria hence seems to be key

287   to electrokinetic control of bacterial deposition and transport. Although other descriptors exist,

288   we used the zeta potentials that were derived from electrophoretic mobility measurements using

289   the standard Smoluchowski theory. Such approach has been described to be adequate and to be a

290   better predictor for bacterial deposition rates than outer surface potentials described by soft

291   particle theory[36].

292 We challenged our observations by reversing the direction of the electric field during deposition

293 experiments of *P. putida* KT2440 and *P. fluorescens* LP6a (Fig. S4, Tables S4 & S5). As

294 expected, the resulting F_{net} differed due to changed relative direction of the EOF and the

295 hydraulic flow in the columns. However, no significant changes in the overall deposition and

296 transport during breakthrough of the two bacterial strains were observed (Fig. S4) with data

297 fitting well to Fig. 2.

298

299 **Relevance for Environmental and Biotechnological Application**

300 Our results suggest that DC electric fields effects may be used to control bacterial deposition and

301 transport in immersed porous media, however, material heterogeneity will have to be considered

302 before any practical applications. Such effects may help to increase the retention of unwanted

303 bacteria in drinking water purification systems[37,38] or, vice versa, to reduce biofouling[39–41] and

304 biocorrosion[42] in technical systems. Our data further show that both F_{EOF} and F_{EP}, act on

305 bacterial deposition at extents depending on the $\left| F_{EOF} / F_{EP} \right|$ and ζ_C / ζ_{bac} ratios, respectively

306 (Fig. 2). Increasing the surface charge of the collector supports the deposition of bacteria (or any

307 other colloid) and may promote desired biofilm formation (e.g. in water clean-up systems), while

308 reduction of ζ_C / ζ_{bac} reduces bacterial deposition and, hence, biofilm formation in technical

309 systems where it is undesired (Fig. 2). In our study shifts of ζ_C coincided with electrokinetically-

310 induced changes of the deposition efficiency due to priming of the collector surface to more

311 negative zeta potentials (Table 1); such priming due to continuous deposition of bacteria during

312 percolation has also been described earlier[20]. Tailor-made (i.e. dynamic and possibly reversible)

313 changes of ζ_C hence may be applied in technical applications in order to find solutions for the

314 wanted ζ_C / ζ_{bac} ratios and bacterial deposition, respectively. Drivers of zeta potential variation

315   such as material properties, ionic strength, and pH then become available to steer electric field

316   effects to the aimed direction. For instance, priming of the collector (e.g. with highly charged

317   materials or solutes) will support the deposition of bacteria (or any other colloid) and promote

318   wanted biofilm formation. In drinking water purification systems, with typical low ionic strength

319   (< 10 mM[43]) and neutral pH, the collector matrices (i.e. ion-exchange resins, activated carbon,

320   etc.) typically are highly charged (ζ_C of ca. -50 mV), and high ζ_C / ζ_{bac} ratios are relatively easy

321   to achieve. This may lead to increased bacterial deposition, increased removal of microbial

322   pathogens and, hence, a promotion of drinking water safety. On the other hand, reduction of

323   ζ_C / ζ_{bac} reduces bacterial deposition and hence, biofilm formation in technical systems (Fig. 2).

324   Several DC-based approaches have been proposed to influence bacteria-electrode surface

325   interactions: some studies aimed at disrupting biofilm formation on electrodes by applying a

326   biocidal current[20] while others used electrokinetic approaches for better application to

327   biofilm[35,44]. Weak DC electric fields have not been found to negatively affect bacterial

328   physiology and activity[20,45], nor to change bacterial physico-chemical surface properties relevant

329   for adhesion and transport[20]. Applying DC fields also opens possibilities for enhanced bacterial

330   transport in porous natural matrices. Investigations have found that in the natural soil system

331   where typical zeta potential distribution ranges of bacteria (-5 to -48 mV[46,47]) and matrices (0 to -

332   54 mV[48–50]) are relatively wide, the two different effects of electric fields exist at the same time

333   regarding the ζ_C / ζ_{bac} distribution. For the situations $\zeta_C / \zeta_{bac} > 1.29$ (i.e. $\left| F_{EOF} \right| > \left| F_{EP} \right|$),

334   DC fields enhance the deposition of bacterial in porous matrices, however, the strong F_{EOF} may

335   enhance the desorption and migration of contaminants[51], and thus may also bridge the physical

336   distance between bacterium and contaminants to further enhance bioremediation. On the other

337   hand, at $\zeta_C / \zeta_{bac} < 1.29$ (i.e. $\left| F_{EOF} \right| < \left| F_{EP} \right|$), DC fields may enhance the transport of bacteria

through porous media to reach contaminants adsorbed on matrices, and enhance bioremediation. In electrokinetically-managed natural and manmade ecosystems knowledge of the electroosmotic flow and electrophoresis hence allows for better control of microbial deposition transport in porous media.

Associated Content

Supporting information containing text, 6 tables and 5 figures is provided.

Acknowledgements

References

(1) Gavin, L.; Gillian, D. L. *Microbial Biofilms: Current Research and Applications*; Caister Academic: Norfolk, U.K., 2012.

(2) Worrich, A.; König, S.; Banitz, T.; Centler, F.; Frank, K.; Thullner, M.; Harms, H.; Miltner, A.; Wick, L. Y.; Kästner, M. Bacterial Dispersal Promotes Biodegradation in Heterogeneous Systems Exposed to Osmotic Stress. *Front. Microbiol.* **2016**, *7*, art. 1214.

(3) Meng, F.; Zhang, S.; Oh, Y.; Zhou, Z.; Shin, H.-S.; Chae, S.-R. Fouling in Membrane Bioreactors: An Updated Review. *Water Res.* **2017**, *114*, 151–180.

(4) PARKER, C. Species of Sulphur Bacteria Associated with the Corrosion of Concrete. *Nature* **1947**, *159* (4039), 439–440.

(5) Torkzaban, S.; Bradford, S. A.; Walker, S. L. Resolving the Coupled Effects of Hydrodynamics and DLVO Forces on Colloid Attachment in Porous Media. *Langmuir* **2007**, *23* (19), 9652–9660.

(6) Martin, R. E.; Bouwer, E. J.; Hanna, L. M. Application of Clean-Bed Filtration Theory to Bacterial Deposition in Porous Media. *Environ. Sci. Technol.* **1992**, *26* (5), 1053–1058.

(7) Velasco-Casal, P.; Wick, L. Y.; Ortega-Calvo, J.-J. Chemoeffectors Decrease the Deposition of Chemotactic Bacteria during Transport in Porous Media. *Environ. Sci. Technol.* **2008**, *42* (4), 1131–1137.

(8) *Particle Deposition and Aggregation: Measurement, Modelling and Simulation*; Elimelech, M., Ed.; Colloid and surface engineering series; Butterworth-Heinemann: Oxford, 1998.

(9) Redman, J. A.; Walker, S. L.; Elimelech, M. Bacterial Adhesion and Transport in Porous Media: Role of the Secondary Energy Minimum. *Environ. Sci. Technol.* **2004**, *38* (6), 1777–1785.

(10) Song, L.; Johnson, P. R.; Elimelech, M. Kinetics of Colloid Deposition onto Heterogeneously Charged Surfaces in Porous Media. *Environ. Sci. Technol.* **1994**, *28* (6), 1164–1171.

(11) Elimelech, M.; Chen, J. Y.; Kuznar, Z. A. Particle Deposition onto Solid Surfaces with Micropatterned Charge Heterogeneity: The "Hydrodynamic Bump" Effect. *Langmuir* **2003**, *19* (17), 6594–6597.

(12) Bhattacharjee, S.; Ko, C.-H.; Elimelech, M. DLVO Interaction between Rough Surfaces. *Langmuir* **1998**, *14* (12), 3365–3375.

(13) Hermansson, M. The DLVO Theory in Microbial Adhesion. *Colloids Surf. B Biointerfaces* **1999**, *14* (1–4), 105–119.

(14) Simoni, S. F.; Bosma, T. N. P.; Harms, H.; Zehnder, A. J. B. Bivalent Cations Increase Both the Subpopulation of Adhering Bacteria and Their Adhesion Efficiency in Sand Columns. *Environ. Sci. Technol.* **2000**, *34* (6), 1011–1017.

(15) Hu, Y.; Werner, C.; Li, D. Electrokinetic Transport through Rough Microchannels. *Anal. Chem.* **2003**, *75* (21), 5747–5758.

(16) Masliyah, J. H.; Bhattacharjee, S. *Electrokinetic and Colloid Transport Phenomena*; John Wiley & Sons: New Jersey, 2006.

(17) Pennathur, S.; Santiago, J. G. Electrokinetic Transport in Nanochannels. 1. Theory. *Anal. Chem.* **2005**, *77* (21), 6772–6781.

(18) Kuo, C.-C.; Papadopoulos, K. D. Electrokinetic Movement of Settled Spherical Particles in Fine Capillaries. *Environ. Sci. Technol.* **1996**, *30* (4), 1176–1179.

(19) Kirby, B. J.; Hasselbrink, E. F. Zeta Potential of Microfluidic Substrates: 1. Theory, Experimental Techniques, and Effects on Separations. *ELECTROPHORESIS* **2004**, *25* (2), 187–202.

398 (20) Qin, J.; Sun, X.; Liu, Y.; Berthold, T.; Harms, H.; Wick, L. Y. Electrokinetic Control of Bacterial
399   Deposition and Transport. *Environ. Sci. Technol.* **2015**, *49* (9), 5663–5671.

400 (21) DeFlaun, M. F.; Condee, C. W. Electrokinetic Transport of Bacteria. *J. Hazard. Mater.* **1997**, *55* (1–
401   3), 263–277.

402 (22) Secord, E. L.; Kottara, A.; Van Cappellen, P.; Lima, A. T. Inoculating Bacteria into Polycyclic
403   Aromatic Hydrocarbon-Contaminated Oil Sands Soil by Means of Electrokinetics. *Water. Air. Soil*
404   *Pollut.* **2016**, *227* (8), 288.

405 (23) Haber, S. Deep Electrophoretic Penetration and Deposition of Ceramic Particles inside Impermeable
406   Porous Substrates. *J. Colloid Interface Sci.* **1996**, *179* (2), 380–390.

407 (24) Wick, L. Y.; Mattle, P. A.; Wattiau, P.; Harms, H. Electrokinetic Transport of PAH-Degrading
408   Bacteria in Model Aquifers and Soil. *Environ. Sci. Technol.* **2004**, *38* (17), 4596–4602.

409 (25) Nelson, K. E.; Weinel, C.; Paulsen, I. T.; Dodson, R. J.; Hilbert, H.; Martins dos Santos, V. A. P.;
410   Fouts, D. E.; Gill, S. R.; Pop, M.; Holmes, M. Complete Genome Sequence and Comparative
411   Analysis of the Metabolically Versatile Pseudomonas Putida KT2440. *Environ. Microbiol.* **2002**, *4*
412   (12), 799–808.

413 (26) Furuno, S.; Remer, R.; Chatzinotas, A.; Harms, H.; Wick, L. Y. Use of Mycelia as Paths for the
414   Isolation of Contaminant-Degrading Bacteria from Soil: Use of Mycelia as Paths for the Isolation of
415   Bacteria. *Microb. Biotechnol.* **2012**, *5* (1), 142–148.

416 (27) Foght, J. M.; Westlake, D. W. Transposon and Spontaneous Deletion Mutants of Plasmid-Borne
417   Genes Encoding Polycyclic Aromatic Hydrocarbon Degradation by a Strain of Pseudomonas
418   Fluorescens. *Biodegradation* **1996**, *7* (4), 353–366.

419 (28) Achtenhagen, J.; Goebel, M.-O.; Miltner, A.; Woche, S. K.; Kästner, M. Bacterial Impact on the
420   Wetting Properties of Soil Minerals. *Biogeochemistry* **2015**, *122* (2–3), 269–280.

421 (29) Goldman, A. J.; Cox, R. G.; Brenner, H. Slow Viscous Motion of a Sphere Parallel to a Plane
422   Wall—II Couette Flow. *Chem. Eng. Sci.* **1967**, *22* (4), 653–660.

423 (30) Probstein, R. F. *Physicochemical Hydrodynamics: An Introduction*; John Wiley & Sons, 2005.

424 (31) Ghosal, S. Fluid Mechanics of Electroosmotic Flow and Its Effect on Band Broadening in Capillary
425   Electrophoresis. *ELECTROPHORESIS* **2004**, *25* (2), 214–228.

426 (32) Shi, L.; Müller, S.; Harms, H.; Wick, L. Y. Factors Influencing the Electrokinetic Dispersion of
427   PAH-Degrading Bacteria in a Laboratory Model Aquifer. *Appl. Microbiol. Biotechnol.* **2008**, *80* (3),
428   507–515.

429 (33) Solomentsev, Y.; Böhmer, M.; Anderson, J. L. Particle Clustering and Pattern Formation during
430   Electrophoretic Deposition: A Hydrodynamic Model. *Langmuir* **1997**, *13* (23), 6058–6068.

431 (34) Locke, B. R. Electrophoretic Transport in Porous Media: A Volume-Averaging Approach. *Ind. Eng.*
432   *Chem. Res.* **1998**, *37* (2), 615–625.

433 (35) Hunter, R. J. *Zeta Potential in Colloid Science: Principles and Applications*, 3. print.; Colloid
434   science; Academic Pr: London, 1988.

435 (36) Alexis J. de Kerchove; Menachem Elimelech. Relevance of Electrokinetic Theory for "Soft"
436   Particles to Bacterial Cells: Implications for Bacterial Adhesion. *Langmuir* **2005**, *21* (14), 6462–
437   6472.

438 (37) Besra, L.; Liu, M. A Review on Fundamentals and Applications of Electrophoretic Deposition
439   (EPD). *Prog. Mater. Sci.* **2007**, *52* (1), 1–61.

440 (38) T, P. A.; Rolf, B.; J, B. H. Controlled Electrophoretic Deposition of Bacteria to Surfaces for the
441   Design of Biofilms. *Biotechnol. Bioeng.* **2000**, *67* (1), 117–120.

442   (39) Zumbusch, P. v; Kulcke, W.; Brunner, G. Use of Alternating Electrical Fields as Anti-Fouling
443   Strategy in Ultrafiltration of Biological Suspensions – Introduction of a New Experimental
444   Procedure for Crossflow Filtration. *J. Membr. Sci.* **1998**, *142* (1), 75–86.

445   (40) Jagannadh, S. N.; Muralidhara, H. S. Electrokinetics Methods To Control Membrane Fouling. *Ind.*
446   *Eng. Chem. Res.* **1996**, *35* (4), 1133–1140.

447   (41) G, B.; E, O. Reduction of Membrane Fouling by Means of an Electric Field During Ultrafiltration of
448   Protein Solutions. *Berichte Bunsenges. Für Phys. Chem.* **1989**, *93* (9), 1026–1032.

449   (42) Lin; J; Ballim; R. Biocorrosion Control: Current Strategies and Promising Alternatives. *Afr. J.*
450   *Biotechnol.* **2012**, *11* (91), 15736–15747.

451   (43) *Guidelines for Drinking-Water Quality*, 4th ed.; World Health Organization, Ed.; World Health
452   Organization: Geneva, 2011.

453   (44) *Encyclopedia of Membranes*; Drioli, E., Giorno, L., Eds.; Springer Berlin Heidelberg: Berlin,
454   Heidelberg, 2016.

455   (45) Shi, L.; Müller, S.; Loffhagen, N.; Harms, H.; Wick, L. Y. Activity and Viability of Polycyclic
456   Aromatic Hydrocarbon-degrading Sphingomonas Sp. LB126 in a DC-electrical Field Typical for
457   Electrobioremediation Measures. *Microb. Biotechnol.* **2008**, *1* (1), 53–61.

458   (46) Soni, K. A.; Balasubramanian, A. K.; Beskok, A.; Pillai, S. D. Zeta Potential of Selected Bacteria in
459   Drinking Water When Dead, Starved, or Exposed to Minimal and Rich Culture Media. *Curr.*
460   *Microbiol.* **2008**, *56* (1), 93–97.

461   (47) Van Loosdrecht, M. C.; Lyklema, J.; Norde, W.; Schraa, G.; Zehnder, A. J. Electrophoretic
462   Mobility and Hydrophobicity as a Measured to Predict the Initial Steps of Bacterial Adhesion. *Appl.*
463   *Environ. Microbiol.* **1987**, *53* (8), 1898–1901.

464   (48) Stenström, T. A. Bacterial Hydrophobicity, an Overall Parameter for the Measurement of Adhesion
465   Potential to Soil Particles. *Appl. Environ. Microbiol.* **1989**, *55* (1), 142–147.

466   (49) Vane, L. M.; Zang, G. M. Effect of Aqueous Phase Properties on Clay Particle Zeta Potential and
467   Electro-Osmotic Permeability: Implications for Electro-Kinetic Soil Remediation Processes. *J.*
468   *Hazard. Mater.* **1997**, *55* (1–3), 1–22.

469   (50) Yukselen, Y.; Kaya, A. Zeta Potential of Kaolinite in the Presence of Alkali, Alkaline Earth and
470   Hydrolyzable Metal Ions. *Water. Air. Soil Pollut.* **2003**, *145* (1–4), 155–168.

471   (51) Wick, L. Y.; Shi, L.; Harms, H. Electro-Bioremediation of Hydrophobic Organic Soil-Contaminants:
472   A Review of Fundamental Interactions. *Electrochimica Acta* **2007**, *52* (10), 3441–3448.

473

474 **Table 1.** Overview of the bacterial zeta potential and the water contact angles, the zeta potential of the collector surface (glass beads) after

475 bacterial deposition and the calculated clean bed deposition efficiency (α_0; 0 - 2 PV) and the deposition efficiency (α_t) at quasi steady state of

476 the breakthrough curves in absence (no DC) and presence of DC electric fields of varying field strength ($E = 0 - 3$ V cm^{-1}). Please note that

477 quasi steady state of the breakthrough curves is reached at different times for the bacteria analyzed as specified in the footnote to this table.

478

Bacteria name	zeta potential of bacteria	zeta potential of collector surface with bacteria [b]	water contact angle	water contact angle of collector with bacteria [b]	collision efficiency (no DC)	collision efficiency (1 V cm^{-1})	collision efficiency (2 V cm^{-1})	collision efficiency (3 V cm^{-1})
	ζ_{bac}	ζ_{C_t}	Θ_w	Θ_{w_t}	$\alpha_{0,no\ DC}$ [c] $\alpha_{t,no\ DC}$	$\alpha_{0,\ 1.0\ V/cm}$ [bc] $\alpha_{t,\ 1.0\ V/cm}$	$\alpha_{0,\ 2.0\ V/cm}$ [c] $\alpha_{t,\ 2.0\ V/cm}$	$\alpha_{0,\ 3.0\ V/cm}$ [c] $\alpha_{t,\ 3.0\ V/cm}$
	(mV)	(mV)	(degree)	(degree)	($\times 10^{-2}$)	($\times 10^{-2}$)	($\times 10^{-2}$)	($\times 10^{-2}$)
P. putida KT2440	-11 ± 1	-11 ± 3	70 ± 3	25 ± 3	28 (0.95) 0.44 ± 0.04 [d]	25 (0.87) 0.88 ± 0.07 [d]	19 (0.78) 1.89 ± 0.17 [d]	19 (0.84) 3.01 ± 0.13 [d]
R. opacus X9	-18 ± 3	-15 ± 2	62 ± 3	30 ± 2	43 (0.94) 1.01 ± 0.12 [e]	34 (0.90) 1.34 ± 0.26 [e]	24 (0.88) 1.55 ± 0.20 [e]	15 (0.91) 1.68 ± 0.21 [e]
P. fluorescens LP6a [a]	-35 ± 3 [a]	-16 ± 3	46 ± 3	34 ± 5	26 (0.98) 1.7 ± 0.16 [a,f]	19 (0.83) 0.94 ± 0.19 [a,f]	19 (0.98) 0.28 ± 0.03 [a,f]	4 (0.95) 0 ± 0 [a,f]
Sphingomonas sp. S3	-23 ± 2	-15 ± 4	53 ± 5	39 ± 4	38 (0.67) 1.65 ± 0.34 [g]	17 (0.63) 1.48 ± 0.36 [g]	19 (0.81) 1.21 ± 0.29 [g]	12(0.89) 0.98 ± 0.21 [g]

479 [a] data taken from [20]; [b] The ζ_C and Θ_w of clean glass bead collectors were 8 ±1 mV and 21 ± 2°, respectively (cf. Table S6); [c] the values in brackets refer to the coefficient of determination r^2;

480 [d] calculated as average from 5 - 13 PV; [e] calculated as average from 5 - 13 PV; [f] calculated as average from 20 - 25 PV (cf. Fig. S2); [g] calculated as average from 8 - 13 PV.

481

482 **Table 2.** Overview of forces acting on a bacterium at the distance of the secondary minimum for deposition to a clean bed (0 - 2 PV;

483 denominated by the subscript '0') and at quasi steady state of the breakthrough curves (denominated by the subscript 't') in presence and

484 absence of DC electric fields of varying field strength (E = 0 - 3 V cm^{-1}): DLVO interaction force (F_{DLVO}), electroosmotic shear force (F_{EOF}),

485 electrophoretic drag force (F_{EP}), the hydraulic shear force (F_{HF}) and the net force (F_{net}) according to eq. 4.

Bacteria name	DLVO force at distance of 2nd minimum	electroosmotic shear force (per V cm^{-1} electric field strength)	electrophoretic drag force (per V cm^{-1} electric field strength)	hydraulic flow shear force	net force at distance of 2nd minimum (no DC)	net force at distance of 2nd minimum (1 V cm^{-1})	net force at distance of 2nd minimum (2 V cm^{-1})	net force at distance of 2nd minimum (3 V cm^{-1})
	F_{DLVO_0} (F_{DLVO_t})	F_{EOF_0} (F_{EOF_t})	F_{EP}	F_{HF}	$F_{net\_0,\ no\ DC}$ $F_{net\_t,\ no\ DC}$	$F_{net\_0,\ 1\ V/cm}$ $F_{net\_t,\ 1\ V/cm}$	$F_{net\_0,\ 2\ V/cm}$ $F_{net\_t,\ 2\ V/cm}$	$F_{net\_0,\ 3\ V/cm}$ $F_{net\_t,\ 3\ V/cm}$
	(pN)	(pN)	(pN)	(pN)	(pN)	(pN)	(pN)	(pN)
P. putida KT2440	3.26 3.69 [a]	1.36 1.87 [a,b]	-1.45	0.2	3.06 3.49 [a,b]	2.97 3.91 [a,b]	2.88 4.33 [a,b]	2.79 4.75 [a,b]
R. opacus X9	5.61 7.62 [a]	1.36 2.55 [a,c]	-2.37	0.2	5.41 7.42 [a,c]	4.4 7.6 [a,c]	3.39 7.78 [a,c]	2.38 7.96 [a,c]
P. fluorescens LP6a	2.31 1.83 [a]	1.36 2.72 [a,d]	-4.74	0.2	2.11 1.63 [a,d]	-1.27 -0.39 [a,d]	-4.65 -2.41 [a,d]	-8.03 -4.43 [a,d]
Sphingomonas sp. S3	8.19 9.82 [a]	1.36 2.55 [a,e]	-3.03	0.2	7.99 9.62 [a,e]	6.32 9.14 [a,e]	4.65 8.66 [a,e]	2.98 8.18 [a,e]

486 [a] calculated using respective ζ_{C_t} and contact angles of bacteria and bacteria adhered glass beads (cf. Tables S6); [b] calculated based on ζ_{C_t} as average from 5 - 13 PV; [c]

487 calculated based on ζ_{C_t} as average from 5 - 13 PV; [d] calculated based on ζ_{C_t} as average from 20 - 25 PV (cf. Fig. S2); [e] calculated based on ζ_{C_t} as average from 8 - 13 PV.
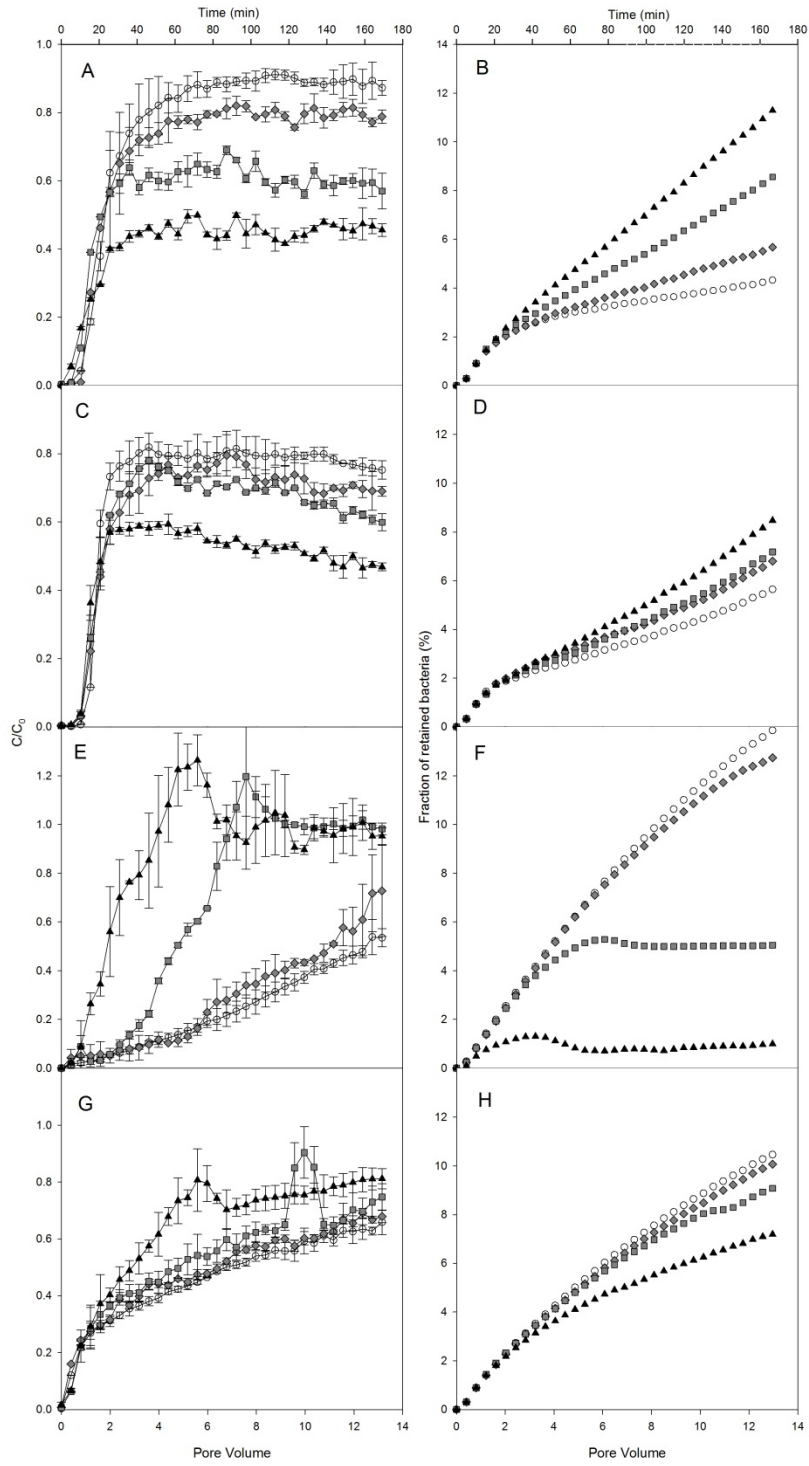
Figure legends

Figure 1. Breakthrough curves (left) and calculated fractions (right) of four bacteria transported through percolation columns packed with glass beads in the absence (open circle) and presence (filled symbols) of DC electric fields of $E = 1.0$ V cm^{-1} (rhomboids), $E = 2.0$ V cm^{-1} (squares) and $E = 3.0$ V cm^{-1} (triangles): *P. putida* KT2440 (Figs. 1A & B), *R. opacus* X9 (Figs. 1C & D), *P. fluorescens* LP6a (Figs. 1E & F), and *Sphingomonas* sp. *S3* (Figs. 1G & H). All data represent averages and standard deviations of triplicate experiments.

Figure 2. Calculated effects of the zeta potential of collector (ζ_C) and bacterial (ζ_{bac}) surfaces on $\left| F_{EOF} / F_{EP} \right|$ ratios (cf. eq. 10). At $\left| F_{EOF} / F_{EP} \right| > 1$ increased and at $\left| F_{EOF} / F_{EP} \right| < 1$ decreased deposition of cells relative to DC-free controls, respectively, is expected. Open and grey filled symbols represent the averages and the standard error (n = 3) of the bacterial surfaces and the initial and late stage zeta potential of glass beads covered by *P. putida* KT2440 (diamonds), *R. opacus* X9 (squares), *P. fluorescens* LP6a (circles), and *Sphingomonas* sp. S3 (triangles). Differences of zeta potential of clean glass beads and glass beads covered with bacteria are statistically significant (p < 0.05) for all bacterial strains.
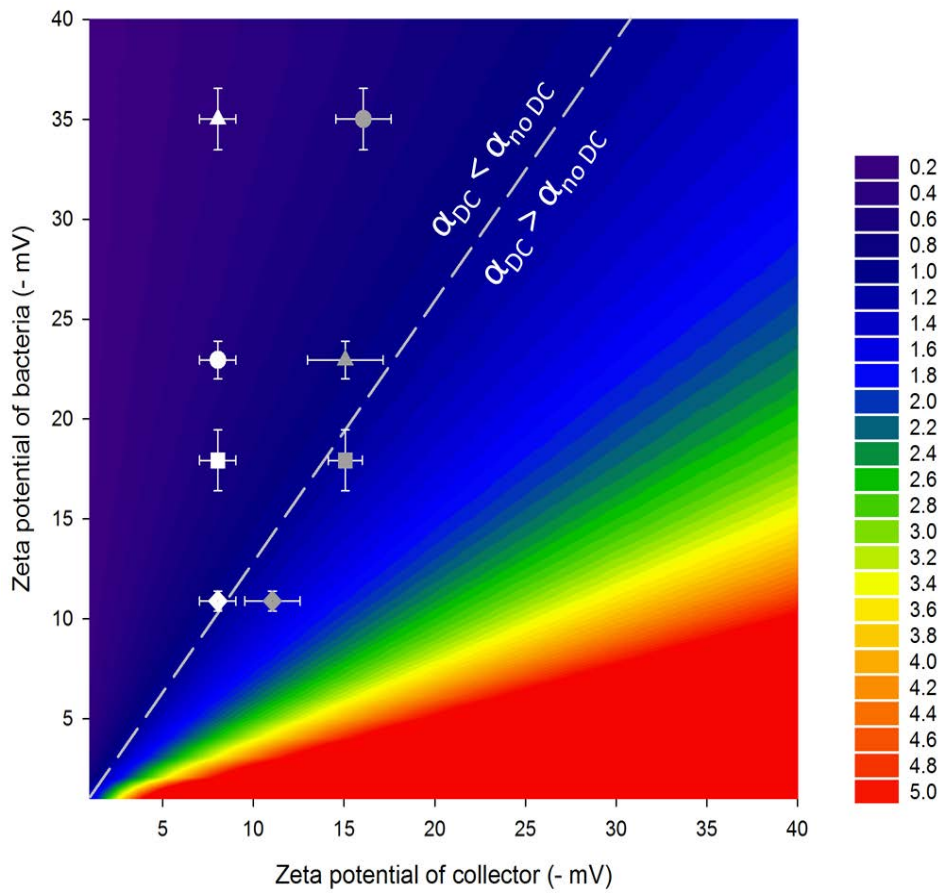
Figure 3. Relative changes of DC-induced net forces acting on a bacterium placed at the secondary and relative changes of the collision efficiency of *P. putida* KT2440 (diamonds), *R. opacus* X9 (squares), *P. fluorescens* LP6a (circles), and *Sphingomonas* sp. S3 (triangles) cells. Open and filled symbols represent relative changes for deposition to clean beds (0 - 2 PV) and at quasi steady state stages of the breakthrough curves (cf. Table 2). Semi-filled symbols represent relative changes in presence of DC fields with reversed polarity applied (i.e. allowing for EOF in direction of the hydraulic flow); top-filled and bottom-filled symbols refer to for deposition to clean beds (0 - 2 PV) and at quasi steady state stages of the breakthrough curves (cf. Table 2).

512

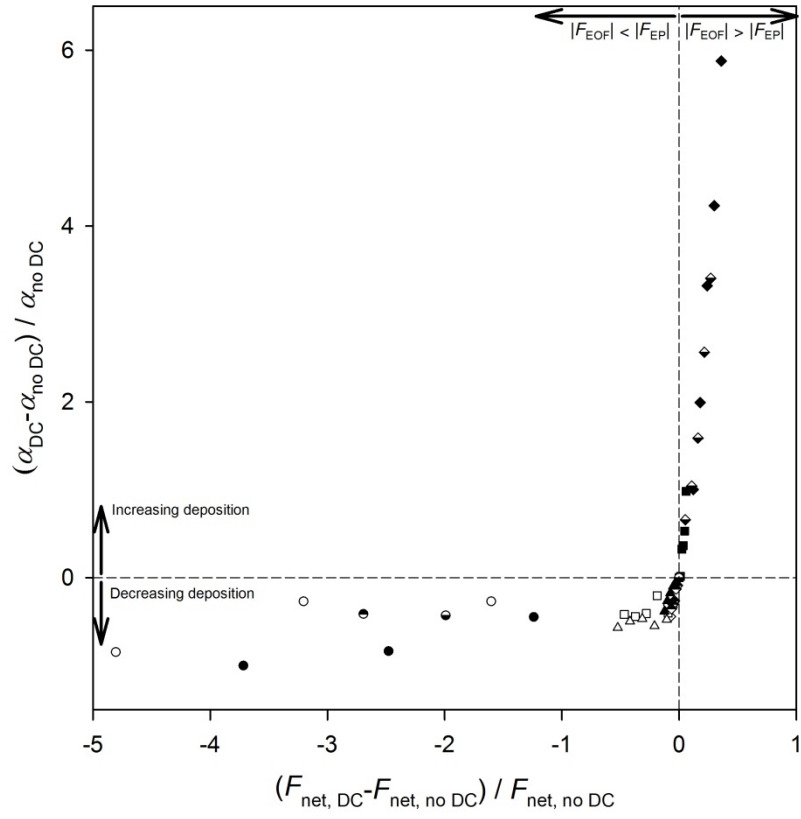**Figure 1**

514

Figure 2

516

517

Figure 3